Gas transfer
Air-water interface
Évaporation
Condensation

Transfert gazeux
Interface air-eau
Évaporation
Condensation

The effect of evaporation and condensation on gas transfer across an air-water interface

P. S. Liss[a], P. W. Balls[a], F. N. Martinelli[a, b], M. Coantic[c]

[a] School of Environmental Sciences, University of East Anglia, Norwich, NR4 7TJ, GB.

[b] Present address: Oil Pollution Division, Warren Spring Laboratory, Stevenage, SG1 2BX, GB.

[c] Institut de Mécanique Statistique de la Turbulence de l'Université d'Aix-Marseille-II, Laboratoire associé au CNRS No. 130, 12, avenue du Général-Leclerc, 13003 Marseille, France.

Received 3/6/80, in revised form 9/12/80, accepted 12/12/80.

ABSTRACT

Experiments to determine the effect on the rate of air-water transfer of oxygen of evaporation and condensation of water molecules have been performed using a laboratory wind-water tunnel in which the wind speed and water and air temperatures, and the humidity of the air can be controlled. Under evaporative conditions there is no measurable enhancement of gas transfer due to destabilization of the near-surface water. In contrast, a reduction in the transfer rate by more than 30 % is observed at intermediate wind speeds under condensing conditions. This retardation can be explained in terms of a stratification parameter. Although, on average, evaporation dominates over condensation at natural air-water interfaces, there are regions and times when the retardation in gas transfer shown here may be of environmental importance.

Oceanol. Acta, 1981, **4**, 2, 129-138.

RÉSUMÉ

Effet de l'évaporation et de la condensation sur le transfert gazeux à travers une interface air-eau.

Des expériences destinées à déterminer l'effet de l'évaporation ou de la condensation des molécules d'eau sur le taux du transfert d'oxygène entre l'air et l'eau ont été effectuées dans une soufflerie air-eau où la vitesse du vent, les températures de l'air et de l'eau, et l'humidité de l'écoulement d'air peuvent être contrôlées. Dans les situations d'évaporation, on n'observe pas d'accroissement mesurable du transfert gazeux sous l'effet de la déstabilisation résultante du film liquide superficiel. Au contraire, une réduction du taux de transfert dépassant 30 % est observée à des vitesses de vent intermédiaires pour les conditions de condensation. Cette diminution peut s'expliquer en fonction d'un paramètre de stratification. Bien que, en moyenne, l'évaporation doive l'emporter sur la condensation à la surface des nappes d'eau naturelles, il existe des endroits et des périodes où cette réduction des échanges gazeux peut avoir des répercussions importantes sur l'environnement.

Oceanol. Acta, 1981, **4**, 2, 129-138.

INTRODUCTION

In the global cycling of many compounds, transfer of natural and man-made gases across the air-sea interface is often of considerable importance (Liss, Slater, 1974). On a smaller scale, exchange of gases occurs across the interface between the atmosphere and coastal waters, lakes and rivers and can probably have important local implications. Despite the significance of such exchanges, the processes controlling air-water transfer rates are still rather poorly understood.

Several attempts have been made to relate air-water gas exchange kinetics to some easily measured physical parameter, such as wind speed, but no such straightforward parameterisation appears to be possible at the present time. For example, although wind tunnel studies clearly indicate that the rate of transfer for gases whose air-water exchange is under liquid phase control increases with wind speed, significant discrepancies exist between different sets of measurements (Downing, Truesdale, 1955; Kanwisher, 1963; Hoover, Berkshire, 1969; Liss, 1973; Broecker *et al.*, 1978; Jähne *et al.* 1979). More critically, field results obtained using the Radon Deficiency Method (Broecker, 1965) as part of the Geosecs programme show little or no relationship between transfer rate and wind speed (Peng *et al.*, 1979; Hasse, Liss, 1980).

The reason for the discrepancy between laboratory and field results has yet to be resolved. It can be hypothesised that, in the field, due to the complexity of the natural environment, factors other than wind speed or parameters directly related to it play important roles and mask the relationships found in wind tunnel studies. The aim of the present study was to investigate some of these suggested other factors by use of experiments performed in a wind tunnel allowing simulation of air-sea interaction processes.

As far as can be ascertained, virtually all the laboratory results to date have been obtained under conditions where there was net evaporation of water from the water surface. However, Hoover and Berkshire (1969) found in their wind tunnel study of air-water CO_2 exchange that if the water temperature was below the dew point of the air above it then transfer was severely inhibited. This led Quinn and Otto (1971) to suggest that the effect may be due to condensation of water on the surface, leading to a decrease in the "normal" evaporation-driven convective motions in the water near the interface, which these authors propose are important in bringing about gas exchange. If such processes are important then it isn't very surprising that in the field the relationship between gas transfer rate and wind speed is not simple, since factors such as air-water temperature difference and relative humidity of the air will also affect the exchange rate.

The principal objective of the present study was to examine the role of evaporation and condensation on the rate of air-water gas transfer. To this end a series of gas exchange experiments were conducted using a wind-water tunnel in which air and water temperatures and air humidity, as well as wind speed, could be accurately controlled. In all the experiments O_2 was used as the gas whose exchange was monitored. As discussed by Liss (1973), the air-water transfer of O_2 is under liquid phase control and its behaviour will almost certainly represent that of most gases of this type.

EXPERIMENTAL PROCEDURE AND DATA PROCESSING

The air-sea interaction simulating facility

The experiments reported here were carried out in 1978 using the smaller of the two air-sea interaction simulating facilities built at IMST, the main elements of which are shown diagramatically in Figure 1. Basically, it is a re-circulating wind-water tunnel, having a working section approximately 8 m long, 0.5 m wide and with an air height and a water depth of around 0.3 m each. Details on the design and performance of the tunnel can be found in Coantic *et al.*, (1969), Pouchain (1970), and Coantic and Favre (1970).

Perhaps the most novel feature of the IMST air-sea interaction facilities is their ability to control not only both air and water temperatures but also the humidity of the air stream. The temperature of the water is regulated by circulating it through hot and cold heat exchangers downstream of the circulation pump (see Fig. 1). The humidity and temperature of the air stream are controlled by passing the flow over large capacity cooling and heating coils and by direct injection of water vapour (where necessary). For better thermal stability, the heat exchangers for both air and water are fed from common large volume supplies of temperature-stabilised hot and cold water.

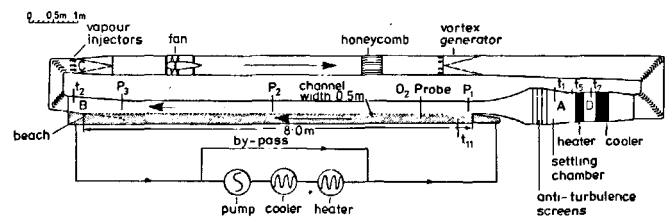

Figure 1

Vertical section through the small air-sea interaction facility at IMST. P_1, P_2 and P_3 mark the positions of the micrometeorological probes. t_1, t_2, t_5, t_7 and t_{11} show the positions of the thermocouple temperature sensors.

Since the experiments depend critically on the ability to control the humidity and temperature in the tunnel, it is necessary to examine how this is achieved. This will be done with the aid of the temperature-specific humidity diagram in Figure 2. Three separate hygrometric situations are illustrated, i. e. net condensation from the air stream onto the water surface; neutral case, where there is practically no net interphase transfer; and net evaporation of vapour from the water surface. In all three cases the air immediately adjacent to the water surface is taken to be at the bulk water temperature (as close to 15°C as possible for all the experiments) and 100% saturated with respect to the water surface.

For the idealised neutral case experiments the bulk air flow is maintained at the same temperature as the water and 100% saturated with water vapour, as shown by the asterisk (*) in Figure 2. Thus there should be no humidity gradient between the water surface and the air stream and no net transfer of water.

The point marked * also represents the hygrometric condition at the water surface for evaporation and condensation experiments. In these the air stream entering the working section of the tunnel (point A on Fig. 1 and 2) contains either too much (condensing case) or too little (evaporation case) water vapour with respect to conditions at the water surface. In traversing the water the air moves towards equilibrium by condensing or evaporating water onto or from the surface, as

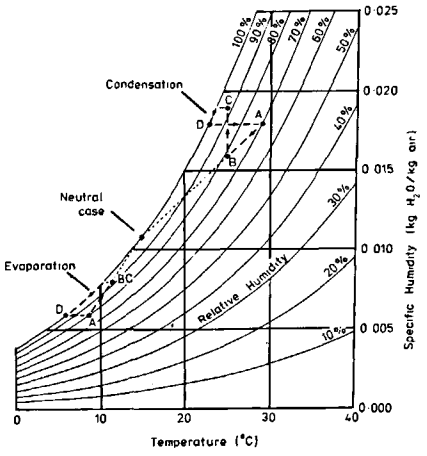

Figure 2
Temperature-specific humidity diagram showing the hygrometric conditions of the air stream at various points in the wind tunnel for evaporative and condensing experiments. Capital letters refer to positions in the wind tunnel shown in Figure 1.

represented by the straight line joining A and the the water surface condition (*) in Figure 2. Since the water surface is only of limited extent full equilibrium is not attained and the air leaving the working section has properties corresponding to point B. For condensation experiments extra vapour is injected at point C leading to increase in the specific humidity with very little effect on temperature (line BC in upper part of Fig. 2). For evaporation experiments points B and C are coincident since no vapour injection is employed. In either case nothing further happens until the air passes through the cooler which lowers the temperature, but whose main function is to remove water vapour by condensation onto the cooling coils. The latter are equipped with a system of gutters which allows the condensed water to be collected for measurement of the bulk evaporation rate (see later). If the cooler/condenser is 100% efficient then the air at point D will be just saturated; because it is slightly less than fully efficient, the actual vapour content generally corresponds to slightly under 100% relative humidity. The air then passes through heating coils (D-A) where its temperature increases without change in specific humidity. As a consequence, the moisture and temperature conditions of the air entering the test section are controlled by the temperatures of the cooler and heater, respectively. In no circumstances is the air stream allowed to become supersaturated (i. e. to plot to the left of the 100% relative humidity curve on Figure 2) since this would result in the formation of mist in the tunnel.

In the evaporative mode it is possible to monitor the efficiency of the air cooling system by comparing the temperature of the air stream as it emerges from the cooling coils (thermocouple t_7) with that measured by a dew point hygrometer positioned on probe P_1 at the entrance to the working section. Theoretically, with 100% cooler efficiency the two temperatures will be identical; any inefficiency being manifested as a lower temperature on t_7 than the dew point measured on P_1. In practice this is not the only cause of discrepancy but the difference between t_7 and P_1 should remain constant throughout an experiment, any increase being, an indication of a malfunction in the cooling system. In practice, the discrepancy was never greater than 0.5°C and was more typically between 0.0 and 0.3°C.

Chemical measurements and data processing

In order to study the rate of oxygen transfer across the air-water interface the water in the working section of the tunnel was first depleted of dissolved O_2 by bubbling pure N_2 gas through it. To encourage efficient de-oxygenation the nitrogen was introduced into the water as several fine streams of bubbles by means of aeration blocks and during the process the return air path in the tunnel was temporarily blanked off. Because of the large volume of water involved it was not possible to reduce the amount of O_2 in the water to less than about 40% of its saturation value, although this deficit proved quite large enough for the experiments to be performed. After de-oxygenation the bubblers were removed from the water and excess N_2 in the air stream flushed out by circulating the air at a relatively high speed for a few minutes (which had the additional advantage of blowing any organic material on the water surface onto the beach at the down wind end of the test section from which it was removed). Following final adjustments to the air and water temperatures and humidity of the air, the rate of increase in the O_2 concentration in the water was monitored as it returned to equilibrium with the normal atmospheric partial pressure of this gas.

Oxygen concentrations in the water were measured at the position indicated in Figure 1 using an EIL Dissolved Oxygen Meter Model 15 A calibrated before and after each experiment. In most of the experiments demineralised water was used, although for experiments 16-23 inclusive this was replaced by tap water.

In the analysis of the oxygen concentration data it is important to be sure that the water is sufficiently homogeneous so that O_2 measurements made at one point are representative of concentrations in the whole water body. Before any experiments were performed tests were made to ascertain the setting of the water circulation pump by-pass system (Fig. 1) required to ensure complete homogeneity of the water in the tank in the absence of wind but with *minimum* disturbance of the water surface since, the main objective being to ascertain the effect of meteorological factors on oxygen transfer, unnecessary mixing (i. e. greater than that required to ensure water homogeneity with no wind) was to be avoided. Once the appropriate setting was found it was used in all subsequent experiments. Measurements of the water drift velocity (no wind) using a miniature propeller flow meter showed it to be less than 1 cm sec^{-1}, except near the surface very close to the entrance to the working section where values of up to 3.5 cm sec^{-1} were recorded.

Provided the water is homogeneous the change in dissolved oxygen concentration with time can be described by the following equation:

$$\frac{dC}{dt} = K \cdot \frac{A}{V} (C_s - C),$$

where C is the oxygen concentration at time t and C_s the saturation concentration, A the area of the free water surface considered flat, and V the volume of water in the tank and circulation system. The transfer velocity, K, is a measure of the rate at which O_2 crosses the air-water interface, i. e. the flux per unit of concentration difference. Integration of the above rate equation gives:

$$\ln \frac{(C_s - C)}{(C_s - C_0)} = -K.t.\frac{A}{V},$$

where C_0 is the oxygen concentration at time $t=0$.
By plotting experimental values of $\ln (C_s - C)$ against t a straight line graph of slope $-K.A/V$ will be obtained. Since V/A is known (34 cm in all the present experiments), the value of K can be readily obtained. A typical plot is shown in Figure 3.

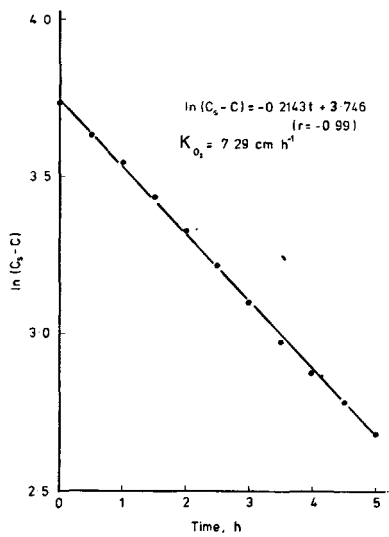

Figure 3
Graph of $\ln (C_s - C)$ *as a function of time for a typical re-oxygenation experiment (No. 23).*

Micrometeorological measurements and data processing

Instrumentation

As indicated on Figure 1, micrometeorological measurements in the air stream could be made using probes at three positions in the tunnel, roughly corresponding to the entrance (P1), mid-point (P2), and exit (P3) of the working section. Air velocity, temperature, and humidity were measured simultaneously by means of a multiprobe comprising a Pitot tube, a thermocouple, and an aspirating pipe leading to a hygrometer. To record vertical profiles, the probe was mounted on a displacement device which allowed it to be positioned at known elevations to an accuracy of 0.02 mm. The dynamic pressure given by the Pitot tube was measured using a Van Essen micromanometer with 0.025 mm reading accuracy. Below 2.5 m sec^{-1}, the dynamic pressure was too small to be measured with sufficient accuracy, so that velocities were determined by hot-wire anemometry (we thank Dr. J. P. Giovanangeli for making these measurements using a previously calibrated 5 μm wire and a DISA 55 M 05 constant-temperature unit). Chromel-constantan 0.5 mm diameter thermocouples were used in the micrometeorological probe, as well as to measure temperatures at the points shown in Figure 1. The thermocouple cold junctions were kept at 0°C in an ice-bath, and the voltages developed (60 μ V/°C) were recorded on a 12 channel MECI Speedomax recording potentiometer, with 2 mV full-scale sensitivity. Humidity measurements were performed by means of an automatic Peltier effect dew-point hygrometer (E.G. and G. Cambridge System Model 137-C 3). The guaranteed absolute accuracy of this instrument is ±0.2°C dew-point, but, when carefully used, its short-term repeatability is a few hundredths of a degree. Free stream values for wind velocity, temperature and dew-point of the air were all measured using Probe 1 at a height of 17 cm above the water surface at the entrance to the working section. For further details of the instrumentation used, see Selva (1978).

Data Processing

It is required to compute the interfacial shear stress (τ_0) as well as the heat (Q_0) and water vapour (J_0) fluxes from the measured wind velocity ($\overline{U}$), température ($\overline{\theta}$) and specific humidity ($\overline{C}$) distributions as a function of elevation (z) above the water surface. For the present experiments, this can be done in three different ways (see e. g. Resch, Selva, 1979):

– The "profile method" takes advantage of the fact that, over a certain range of elevations, the above distributions obey the logarithmic relationships:

$$\overline{U}(z) - \overline{U}_0 = U_*/\varkappa . \ln (z/z_0),$$

$$\overline{\theta}(z) - \overline{\theta}_0 = \theta_* Pr_t/\varkappa . \ln (z/z_{0\theta}),$$

$$\overline{C}(z) - \overline{C}_0 = C_* Sc_t/\varkappa . \ln (z/z_{0c}),$$

where $U_* = (\tau_0/\rho)^{1/2}$ is the so-called "friction velocity", $\theta_* = -Q_0/\rho C_p U_*$, $C_* = -J_0/\rho U_*$ are reference temperature and specific humidity respectively, ρ and C_p are the specific mass and heat of air (1.2 kg m^{-3} and 10^3 J kg^{-1} K^{-1} respectively), $\varkappa$ is von Karman's constant (taken as 0.40), Pr_t and Sc_t are the Prandtl and Schmidt numbers for turbulence (both taken as equal to 0.75), and the z_0 *s* are integration constants related to the roughness of the interface. As shown by Figure 4, the measured profiles clearly show, for low as well as high wind speeds, a logarithmic region, from the slope of which τ_0, Q_0, and J_0 were estimated (the beginning of the viscous zone very close to the surface can be seen at low wind speeds, e. g. Fig. 4 *a*).

– The "integral method" uses the exit profiles of velocity, temperature, and humidity to compute the amounts of heat and water vapour which have been introduced into or removed from the boundary layer over the length L of the water channel (8 m). Q_0 and J_0 are thus obtained from the formulae:

$$Q_0 = \rho C_p/L \int_0^{\delta} \overline{U}(z)(\overline{\theta}(z) - \theta_e)\, dz,$$

$$J_0 = \rho/L \int_0^{\delta} \overline{U}(z)(\overline{C}(z) - C_e)\, dz,$$

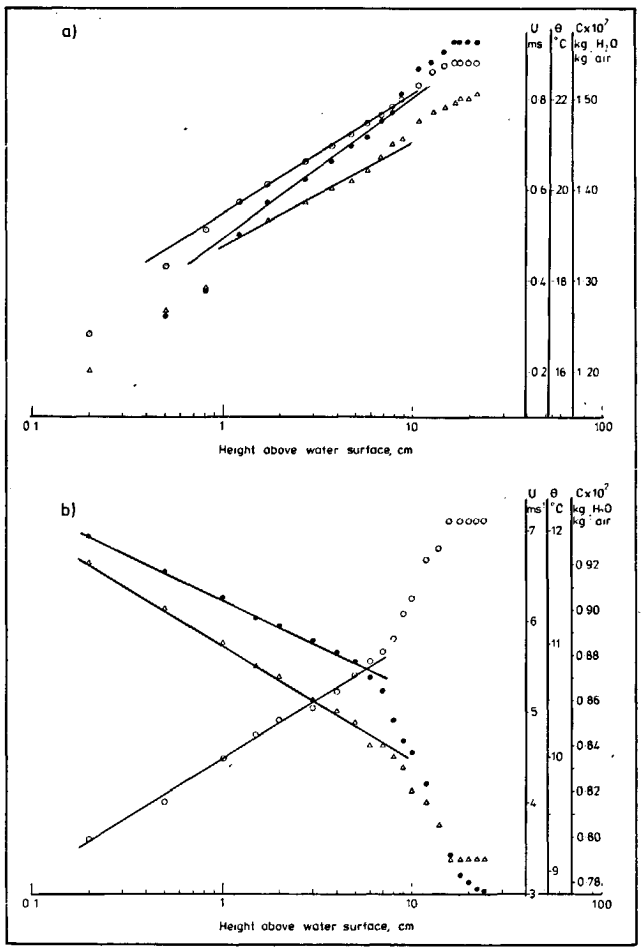

← Figure 4
Wind velocity (⊙), air temperature (Δ) and specific humidity (●) measured at P_3 as a function of height above the water surface. a) Low wind speed experiment (No. 8), $U_e = 0.84\ ms^{-1}$. b) High wind speed experiment (No. 25), $U_e = 7.07\ ms^{-1}$.

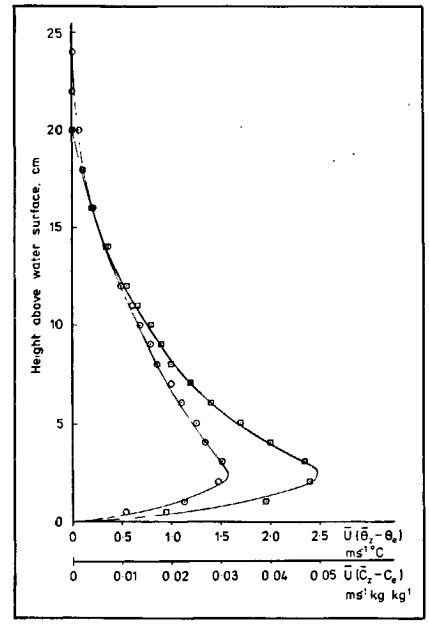

Figure 5
Plots of $\bar{U}(\bar{\theta}_z - \theta_e)$, ⊙, and $\bar{U}(\bar{C}_z - C_e)$, ⊡, measured at P_3 as a function of height above the water surface for experiment No. 4.

wherein δ is the boundary layer thickness at the exit of the working section, and θ_e and C_e the entrance and free-stream temperature and humidity. The integrals were evaluated graphically from plots of the kind shown in Figure 5.

Table I
Summary of experimental results

Type of experiment	Experiment number	Wind velocity U_e (msec^{-1})	Friction velocity U_* smoothed $\times 10^2$ (msec^{-1})	Sensible heat flux Q_0 (Wm^{-2})	Water vapour flux $J_0 \times 10^5$ (kg m^{-2} sec^{-1})	Total heat flux S_0 (Wm^{-2})	O_2 transfer velocity K (cm h^{-1})
E	1	0.36	1.76	0.4	− 0.58	− 14.1	1.89
E	2	0.36	1.76	− 0.7	− 0.49	− 13.0	2.02
C	3	0.36	1.76	20.9	0.62	36.4	1.78
C	4	0.36	1.76	21.4	0.75	40.2	1.90
E	5	0.84	3.93	− 29.3	− 2.23	− 85.1	2.01
E	6	0.84	3.93	− 22.9	− 2.02	− 73.4	2.02
N	7	0.84	3.93	− 5.6	− 0.46	− 17.1	2.06
C	8	0.84	3.93	23.6	1.93	71.9	1.72
C	9	0.84	3.93	33.2	3.23	114.0	1.59
E	10	2.50	11.07	− 47.2	− 4.19	−152.0	3.04
E	11	2.50	11.07	− 26.4	− 2.38	− 85.9	2.92
N	12	2.50	11.07	− 1.6	− 0.38	− 11.1	2.96
C	13	2.50	11.07	76.0	3.05	152.3	2.57
C	14	2.50	11.07	112.0	5.72	255.0	2.31
C	15	2.49	11.07	115.2	7.14	293.7	2.10
C	16	3.12	13.67	107.7	8.66	324.2	3.02
E	17	4.55	19.35	− 64.1	− 5.84	−210.1	11.29
E	18	4.54	19.35	− 72.7	− 5.82	−218.2	9.10
N	19	4.53	19.35	3.8	0.60	18.8	10.26
N	20	4.50	19.35	7.5	1.49	44.8	9.18
C	21	4.49	19.35	232.0	11.82	527.5	5.45
C	22	4.40	19.35	185.0	12.55	498.8	6.45
C	23	4.50	19.35	167.2	12.77	486.5	7.29
E	24	6.99	29.45	− 79.8	− 6.41	−240.1	26.6
E	25	7.01	29.45	− 69.6	− 5.80	−214.6	23.5
N	26	7.03	29.45	1.7	0.00	1.7	25.6
C	27	7.00	29.45	185.7	6.82	356.2	23.2
C	28	7.01	29.45	149.5	14.49	511.8	24.8
E	29	9.20	38.18	−104.6	− 8.90	−327.1	38.2
N	30	9.23	38.18	0.0	− 0.51	− 12.8	37.9
C	31	9.17	38.18	279.0	14.5	641.5	38.4
Column	*a*	*c*	*o*	*z*	*aa*	*bb*	*d*

– The "condensate method" is applicable only to steady-state evaporation experiments. It consists of measuring the flow rate of water which condenses onto the cooler in the wind tunnel, as the return air stream is brought back to its dew point (C-D in Fig. 1 and 2), from which the total rate of evaporation, and therefore J_0, can be readily obtained.

RESULTS

Experiments were conducted at seven different wind speeds in the range 0.36-9.2 m sec^{-1}. For most of the wind velocities there were several runs for each of the conditions, evaporation, condensation, and no net vapour transfer. The full experimental conditions plus raw and processed results are given in the Appendix Table A 1. In text Table 1 the essential results are gathered for convenience.

Column *h* in Table A 1 shows the specific humidity of the air as calculated from its dew point using the Smithsonian Meteorological Tables (1966). The saturation specific humidity given in column *i* is calculated in the same way from the water temperature, i. e. corresponds to the concentration of water vapour in the air immediately adjacent to the water surface, on the assumption that this layer is at equilibrium (i. e. 100% saturated) with the water at the temperature of the aqueous phase. The difference (*h-i*) thus gives the driving force (*j*) for transfer of water vapour between the air and the water; a positive value corresponds to net condensation (C), a negative value indicates net evaporation (E), and a value of zero corresponds to no net flux (neutral case-N). In Table 1 the experiments are classified into one of these three types. As it proved rather difficult to achieve complete neutrality with respect to water vapour gradient, neutral case experiments are defined as those for which the humidity difference (*j*) is $< \pm 12 \times 10^{-4}$ kg H_2O/kg air.

Table A1
Experimental results

Experiment number	Duration (h)	Wind velocity U_e (ms^{-1})	O_2 transfer velocity K ($cm\ h^{-1}$)	Dew point temperature (^0C)	Air temperature (^0C)	Water temperature (^0C)	Air specific humidity $\times 10^2$ (kg H_2O/kg^{-1} air)	Air saturation specific humidity $\times 10^2$ (kg H_2O/kg^{-1} air)	Humidity difference $(h-i) \times 10^2$ (kg H_2O/kg^{-1} air)	Air-water temp. diff. $(f-g)$ ($_0C$)	Profile method (1st approx.) U_* (ms^{-1})	θ_* (^0C)	$C_* \times 10^4$ (kg H_2O/kg^{-1} air)	Friction velocity U_* smoothed $\times 10^2$ (ms^{-1})
1	28	0.36	1.89	10.7	15.1	14.9	0.81	1.07	−0.26	0.2	–	–	–	1.76
2	25	0.36	2.02	10.7	13.8	14.2	0.80	1.02	−0.22	− 0.4	–	–	–	1.76
3	21	0.36	1.78	18.7	26.4	15.2	1.37	1.09	0.28	11.2	–	–	–	1.76
4	23	0.36	1.90	19.4	26.6	15.1	1.43	1.09	0.34	11.5	0.018	1.56	5.55	1.76
5	19	0.84	2.01	4.9	6.8	15.1	0.55	1.08	−0.53	− 8.3	0.043	0.57	3.31	3.93
6	13	0.84	2.02	5.1	7.8	14.3	0.56	1.03	−0.48	− 6.5	–	–	–	3.93
7	6	0.84	2.06	14.0	14.3	15.9	1.03	1.14	−0.11	− 1.6	–	–	–	3.93
8	23	0.84	1.72	20.6	21.8	15.1	1.55	1.09	0.46	6.7	0.043	0.53	3.70	3.93
9	17	0.84	1.59	23.6	25.0	15.6	1.89	1.12	0.77	9.4	–	–	–	3.93
10	6	2.50	3.04	6.3	8.5	14.4	0.60	1.04	−0.44	− 5.9	–	–	–	11.07
11	6	2.50	2.92	10.8	11.4	14.7	0.81	1.06	−0.25	− 3.3	–	–	–	11.07
12	6	2.50	2.96	14.0	14.8	15.0	1.03	1.07	−0.04	− 0.2	–	–	–	11.07
13	6	2.50	2.57	18.6	24.0	14.5	1.37	1.05	0.32	9.5	–	–	–	11.07
14	6	2.50	2.31	21.6	28.3	14.3	1.64	1.04	0.60	14.0	–	–	–	11.07
15	5	2.49	2.10	23.1	29.2	14.8	1.81	1.06	0.75	14.4	–	–	–	11.07
16	5.5	3.12	3.02	22.6	25.2	13.8	1.77	1.00	0.77	11.4	–	–	–	13.67
17	5.5	4.55	11.29	7.8	9.8	14.9	0.67	1.06	−0.39	− 5.1	–	–	–	19.35
18	6	4.54	9.10	7.5	8.8	14.6	0.66	1.05	−0.39	− 5.8	–	–	–	19.35
19	5	4.53	10.26	15.8	15.6	15.3	1.14	1.10	0.04	0.3	–	–	–	19.35
20	6	4.50	9.18	15.7	14.8	14.2	1.13	1.03	0.10	0.6	–	–	–	19.35
21	6	4.49	5.45	23.0	31.9	13.8	1.80	1.00	0.80	18.7	–	–	–	19.35
22	6	4.40	6.45	24.7	30.0	14.9	1.92	1.06	0.86	15.1	–	–	–	19.35
23	5	4.50	7.29	23.8	27.9	14.5	1.90	1.04	0.86	13.4	–	–	–	19.35
24	3	6.99	26.6	8.7	9.4	14.0	0.71	1.02	−0.31	− 4.6	–	–	–	29.45
25	3	7.01	23.5	10.6	11.1	15.1	0.81	1.09	−0.28	− 4.0	0.222	0.28	0.93	29.45
26	3.5	7.03	25.6	15.0	15.1	15.0	1.08	1.08	0.00	0.1	–	–	–	29.45
27	3	7.00	23.2	20.1	27.0	16.3	1.51	1.18	0.33	10.7	0.389	0.66	4.07	29.45
28	3	7.01	24.8	22.9	23.7	15.1	1.80	1.10	0.70	8.6	–	–	–	29.45
29	3	9.20	38.2	9.8	10.4	15.3	0.76	1.11	−0.35	− 4.9	–	–	–	38.18
30	3	9.23	37.9	15.6	15.2	15.2	1.12	1.10	0.02	0.0	–	–	–	38.18
31	3	9.17	38.4	22.8	29.2	16.1	1.73	1.16	0.57	13.1	0.358	0.77	–	38.18
Column *a*	*b*	*c*	*d*	*e*	*f*	*g*	*h*	*i*	*j*	*k*	*l*	*m*	*n*	*o*

From the profile measurements taken at the middle and exit of the test section for several of the experiments, reference friction velocity (U_*), temperature (θ_*), and specific humidity (C_*) were computed using the profile method and are given in columns *l*, *m* and *n* of Table Al. Heat and vapour fluxes Q_0, J_0 have been obtained in a number of cases using the integral method (columns *v* and *w*) and for J_0 only using the condensate method (column *t*). Preliminary examination of the data reveals, as expected from the difficulty of such measurements, a quite significant scatter. This led to the adoption of the following smoothing procedure:

1) The present and a number of other determinations of the friction velocity as a function of the free stream velocity in the same wind tunnel have been used to obtain a smoothed relationship between these two variables. For this the friction coefficient (C_f):

$$C_f=(U_*/U_e)^2,$$

has been computed and is plotted against U_e in Figure 6.

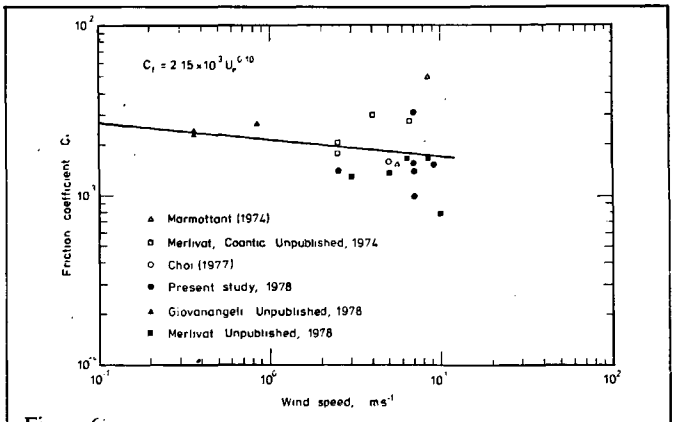

Figure 6

Compilation of results obtained using the small IMST wind-water tunnel for the relationship between friction velocity [expressed as a friction coefficient, $C_f=(U_*/U_e)^2$] and wind speed.

The least squares fit line through the points is:

$$C_f=2.15\times10^{-3}\,U_e^{-0.10},$$

Profile method (2nd approx.)				Condensate method		Integral method				Smoothed values			
Sensible heat flux Q_0 (W m^{-2})	Water vapour flux $J_0\times10^5$ (kg m^{-2} sec^{-1})	Sherwood No. $Sh\times10^{-3}$	Nusselt No. $Nu\times10^{-3}$	Water vapour flux $J_0\times10^5$ (kg m^{-2} sec^{-1})	Sherwood No. $Sh\times10^{-3}$	Sensible heat flux Q_0 (W m^{-2})	Water vapour flux $J_0\times10^5$ (kg m^{-2} sec^{-1})	Sherwood No. $Sh\times10^{-3}$	Nusselt No. $Nu\times10^{-3}$	Sensible heat flux Q_0 (W m^{-2})	Water vapour flux $J_0\times10^5$ (kg m^{-2} sec^{-1})	Total heat flux S_0 (W m^{-2})	Stratification parameter, S_0/U_*^3 (W m^{-5} sec^3)
–	–	–	–	–	–	–	–	–	–	0.4	– 0.58	– 14.1	– 2.59×10^6
–	–	–	–	–	–	–	–	–	–	– 0.7	– 0.49	– 13.0	2.38×10^6
–	–	–	–			–	–	–	–	20.9	0.62	36.4	6.68×10^6
32.9	1.17	0.92	0.91	–	–	21.2	0.55	0.43	0.59	21.4	0.75	40.2	7.36×10^6
– 26.7	– 1.56	0.79	1.02	–	–	–	–	–	–	– 29.3	– 2.23	– 85.1	– 1.40×10^6
–	–	–	–	–	–	–	–	–	–	– 22.9	– 2.02	– 73.4	– 1.21×10^6
–	–	–	–	–	–	–	–	–	–	– 5.6	– 0.46	– 17.1	– 2.82×10^5
25.1	1.75	1.01	1.19	–	–	23.8	1.41	0.82	1.13	23.6	1.93	71.9	1.18×10^6
–	–	–	–	–	–	–	–	–	–	33.2	3.23	114.0	1.88×10^6
–	–	–	–	3.80	2.30	–	–	–	–	– 47.2	– 4.19	–152.0	–11.21×10^4
–	–	–	–	2.33	2.49	– 26.8	– 2.68	2.80	2.55	– 26.4	– 2.38	– 85.9	– 6.33×10^4
–	–	–	–	–	–	–	–	–	–	– 1.6	– 0.38	– 11.1	– 8.18×10^3
–	–	–	–	–	–	–	–	–	–	76.0	3.05	152.3	1.12×10^5
–	–	–	–	–	–	–	–	–	–	112.0	5.72	255.0	1.88×10^5
–	–	–	–	–	–	–	–	–	–	115.2	7.14	293.7	2.17×10^5
–	–	–	–	–	–	–	–	–	–	107.7	8.66	324.2	1.27×10^5
–	–	–	–	–	–	–	–	–	–	– 64.1	– 5.84	– 210.1	– 2.90×10^4
–	–	–	–	7.25	4.96	–	–	–	–	– 72.7	– 5.82	– 218.2	– 3.01×10^4
–	–	–	–	–	–	–	–	–	–	3.8	0.60	18.8	2.59×10^3
–	–	–	–	–	–	–	–	–	–	7.5	1.49	44.8	6.18×10^3
–	–	–	–	–	–	–	–	–	–	232.0	11.82	527.5	7.28×10^4
–	–	–	–	–	–	–	–	–	–	185.0	12.55	498.8	6.88×10^4
–	–	–	–	–	–	–	–	–	–	167.2	12.77	486.5	6.71×10^4
–	–	–	–	10.80	9.30	–	–	–	–	– 79.8	– 6.41	–240.1	– 9.40×10^3
– 98.4	– 3.29	3.13	7.81	8.10	7.71	–	–	–	–	– 69.6	– 5.80	–214.6	– 8.40×10^3
–	–	–	–	–	–	–	–	–	–	1.7	0.00	1.7	6.81×10^2
233.6	14.36	11.6	6.93	–	–	199.0	10.40	8.31	5.87	185.7	6.82	356.2	1.39×10^4
–	–	–	–	–	–	118.8	9.68	4.44	4.86	149.5	14.49	511.8	2.00×10^4
–	–	–	–	14.10	10.74	–	–	–	–	–104.6	–8.90	–327.1	– 5.88×10^3
–	–	–	–	–	–	–	–	–	–	0.0	–0.51	– 12.8	– 2.30×10^2
350.2	–	–	8.49	–	–	–	–	–	–	279.0	14.50	641.5	1.15×10^4
p	*q*	*r*	*s*	*t*	*u*	*v*	*w*	*x*	*y*	*z*	*aa*	*bb*	*cc*

which leads to the empirical relationship:

$U_* = 0.0464\, U_e^{0.95}$.

The smoothed values for U_* are given in column *o*.

2) Using the above smoothed values for U_* and the experimentally determined values of θ_* and C_*, Q_0 and J_0 have been re-calculated and are given in columns *p* and *q*.

3) From all the experimental values for Q_0 (columns *p* and *v*) and J_0 (columns *q*, *t* and *w*) dimensionless heat and mass transfer coefficients (Nusselt and Sherwood Numbers, respectively) have been calculated:

$Nu = Q_0 L/\rho C_p \alpha \Delta t$,

$Sh = J_0 L/\rho D \Delta C$,

where α and D are the molecular diffusivities for heat and water vapour in air (21×10^{-6} and 25×10^{-6} m^2 sec^{-1}, respectively).

As is well known from similarity considerations, these two dimensionless numbers should be practically the same function of the length Reynolds Number:

$Re = U_e L/\nu$,

where ν is the kinematic viscocity of air (1.5×10^{-6} m^2 sec^{-1}). The results obtained are plotted in log-log co-ordinates on Figure 7, for which the following best-fit expression has been calculated:

$Nu = Sh = 0.063\, Re^{0.752}$.

From this relationship, the defining equations for Re, Nu and Sh, and the velocities, temperatures and humidity differences measured during each experiment (columns *c*, *k* and *j*), smoothed values of Q_0 and J_0 have been re-calculated and are given in columns *z* and *aa*, together with the final total (i. e. sensible plus latent) interfacial heat flux S_0 (column *bb*):

$S_0 = Q_0 + L_0 J_0$,

where L_0 is the latent heat of evaporation of water (2.48×10^6 J kg^{-1}).

Values for the transfer velocity for oxygen were calculated according to the procedure described earlier and are given in column *d* of Table A1. From a preliminary inspection of the data it is apparent that, except at the lowest and highest wind speeds, values of

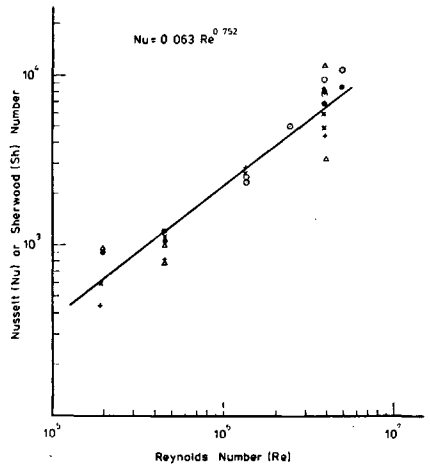

Figure 7

Nusselt (Nu) and Sherwood (Sh) Numbers plotted against Reynolds Number. ● *Nu-profile method,* × *Nu-integral method;* Δ *Sh-profile method,* + *Sh-integral method,* ⊙ *Sh-condensate method.*

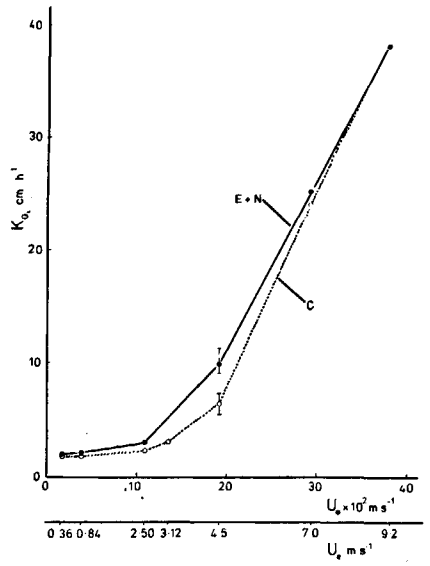

Figure 8

Oxygen transfer velocity as a function of friction velocity and wind speed. Mean of results for: evaporative (E) and neutral (N) case experiments (●), condensing (C) experiments (O). The maximum and minimum values for each of the two groups of results are shown for $U_* = 19.35 \times 10^{-2}\, ms^{-1}$.

the oxygen transfer velocity are significantly lower under condensing conditions than those for evaporative and neutral case experiments. For this reason, in plotting Figure 8, which shows the relationship between transfer velocity and friction velocity (and wind speed), averages have been taken of the results of the condensing (C) and neutral plus evaporative (N+E) experiments, treated as two separate groups. As well as the average data, the maximum and minimum values for each of the two groups are given for the experiments where $U_* = 19.35 \times 10^{-2}$ m sec^{-1}. This range reveals a significant lack of reproducibility between experiments, in spite of the quite small apparent uncertainty for an individual experiment (see Fig. 3).

DISCUSSION

From Figure 8 it is clear that at a given wind speed, in the approximate range 1-7 m sec^{-1}, the oxygen transfer velocity is significantly reduced under condensing as compared with evaporative or neutral conditions. The maximum measured effect was at a wind speed of 4.5 m sec^{-1} where condensing conditions produced a drop of 36% as compared to evaporative and neutral conditions.

The present results are in general agreement with the condensing effect noted by Hoover and Berkshire (1969) in their study of air-water transfer of CO_2. From the graph given in Appendix IV of Hoover (1966) we calculate the condensation effect to be about 30%. In these experiments the effect was an unwanted artefact which was eliminated by ensuring that the water temperature was always above the dew point of the air. As far as we are aware, ours is the first attempt at a systematic study of the role of condensation on air-water gas transfer.

Although the present experiments reproduce the effect observed by Hoover and Berkshire (1969) they do not

provide evidence for the interpretation given by Quinn and Otto (1971), i. e. that evaporative cooling produces mixing in the near surface water which then enhances gas exchange. The results in Table 1 show no significant increase in the transfer velocity, at a fixed wind speed, as the conditions change from neutral to intermediate to high evaporation, as one might expect if evaporatively driven mixing is important. Not even at the lowest wind speed used in the experiments, where mixing of the surface water by wind induced turbulence will be least, is the effect postulated by Quinn and Otto observed. It is, of course, possible that any effect at low wind speeds is masked by mixing of the water produced by the pump used to circulate the water in the tank. Indeed, the levelling off of the curve in Figure 8 at low wind speed to become almost parallel with the x-axis could be due to such mixing producing a certain minimum value for the transfer velocity. If this is the case then it is not possible to say definitely that convective effects are unimportant at low wind speeds, but on the other hand the present experiments cannot be taken as evidence that they are. In any case, even if such effects can be shown to be significant under quiescent conditions their environmental relevance will be doubtful since at natural air-water interfaces conditions will generally by too turbulent for them to be apparent.

The levelling of the transfer velocity versus friction velocity curve, noted above, is in contradiction to the linear decrease to zero at $U_* = 0$ one can predict from models wherein the transfer mechanisms across the interfacial liquid layer are taken as equivalent to the ones close to a solid smooth wall (e. g. Deacon, 1977). It should be noted that most of the available experimental results at wind speeds less than 2 m sec^{-1} do exhibit such a levelling – the asymptotic value varying between 1 and 2 cm hr^{-1} (Downing, Truesdale, 1955; Kanwisher, 1963; Hoover, Berkshire, 1969). As indicated above, it is possible to assume that the finite limiting transfer velocity reflects mixing induced by the water circulation systems. In the present experiments, we assume that, in view of the very similar values for the transfer velocity, the additional mixing due to the wind is practically zero for the two lowest wind speed condensing experiments and thus estimate the minimum limiting value from the average of the observed transfer velocities as 1.75 cm hr^{-1} (K min.).

In order to try to explain the observed reduction in transfer velocity under condensing conditions we can make use of the theory of density stratified turbulent flows to attempt to correlate the relative change in transfer rates with a suitable stratification parameter.

For the transfer of a scalar contaminant with a high Schmidt Number (in the present case dissolved O_2) close to an interface (here the water-air boundary) the transfer velocity can be viewed as a parameter which describes the ability of turbulent motions to propagate very close to the interface with the result that turbulent diffusion overwhelms molecular transport (e. g. Coantic, 1980). It is well known in a density-stratified environment the changes in the turbulence level and structure depend on the relative importance of the rate of buoyant production or destruction of turbulent energy and the rate of mechanical generation of turbulent energy from the kinetic energy of the mean flow. The former is known to be expressed by the term $\rho g \beta \overline{\theta' w'}$, where g is the acceleration due to gravity, β is the coefficient of thermal expansion of water, and $\overline{\theta' w'}$ is the turbulent heat flux divided by ρC_p. The latter is given by $-\rho \overline{u' w'} \partial \bar{u}/\partial z$, i. e. the product of the turbulent Reynolds stress and the mean velocity shear. These two expressions combine to give the fundamental stratification parameter known as the flux Richardson Number (e. g. Monin, Yaglom, 1971):

$$R_f = g \beta \overline{\theta' w'} / \overline{u' w'} \frac{\partial \bar{u}}{\partial z}.$$

In the present case the stabilising effect of the surface heating due to condensation and heat transfer at the water surface will then have to be correlated in terms of an appropriate Richardson Number. The numerator will clearly be proportional to the total air-water heat flux (S_0), as defined previously. The factor $\overline{u' w'}$ in the denominator will be proportional to the friction velocity squared. Use is then made of the classical assumption that there is no stress discontinuity across the air-water interface, with the result that the friction velocity on the water side, U_{*w}, is equal to the air friction velocity times $(\rho \text{air}/\rho \text{water})^{1/2}$. Various experiments (e. g. Shemdin, 1972) have shown that wind drift currents in the uppermost water layers obey the classical logarithmic distribution. As a consequence the current shear, $\partial \bar{u}/\partial z$, should be proportional to U_{*w}/Kz, i. e. at a given depth proportional to U_*. The appropriate stratification parameter is thus S_0/U_*^3. This quantity has been calculated for the present data set and is given in column *cc* of Table A 1. The transfer velocity data have been processed as follows: 1) to eliminate the effect of mixing due to the pump system the asymptotic value of the transfer velocity (K min) has been substracted from all the transfer velocity data; 2) for each wind velocity an average value for K_{E+N} has been taken. In the case of wind speed 3.12 m sec^{-1}, where E + N data are lacking, an estimate of K under these conditions has been made by means of a smoothed curve through the data points for other wind speeds; 3) individual values of the ratio $R = (K_c - K_{min})/(\overline{K_{E+N}} - K_{min})$ have been calculated for each condensing experiment and are plotted against the stratification parameter (S_0/U_*^3) in Figure 9. There

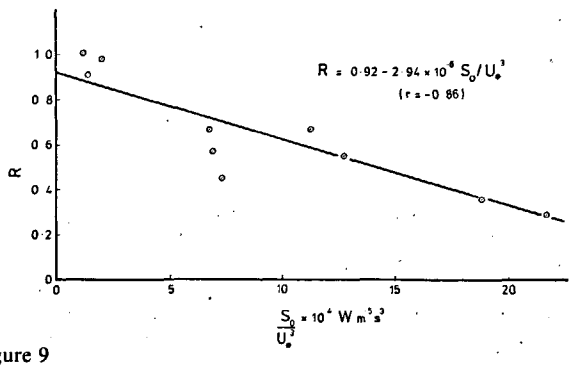

Figure 9

Ratio $(R = K_c - K_{min}/\overline{K_{E+N}} - K_{min})$ *of* O_2 *transfer velocities under condensing and evaporative plus neutral conditions (results corrected for effect of water circulation pump by subtraction of* K_{min}*) plotted against the stratification parameter* S_0/U_*^3.

appears to be a reasonable relationship between R and S_0/U_*^3, the least square line for the plotted points being $R = 0.92 - 2.94 \times 10^{-6} S_0/U_*^3$ ($r = -0.86$).

The possibility that $\partial\bar{u}/\partial z$ could be proportional not to U_* but to U_*^2 (as in the viscous sublayer close to a smooth surface) was investigated, leading to the alternative stratification parameter S_0/U_*^4. However, the relationship between this alternative parameter and R turned out to be much less clear, the least square line being $R = 0.80 - 2.67 \times 10^{-7} S_0/U_*^4$ ($r = -0.67$), i. e. having a lower correlation coefficient and a projected intercept further from the tie-point ($R = 1.00$ when $S_0/U_*^n = 0$) than the original parameter S_0/U_*^3.

ENVIRONMENTAL IMPLICATIONS

Two conclusions may be drawn concerning the environmental importance of the results presented here.

The absence of any observable enhancement of the rate of oxygen transfer as the hygrometric conditions change from neutral to increasing degrees of evaporation implies that convective mixing of the surface water due to evaporative cooling is not a quantitatively important process, at least under the experimental conditions used here, where any effect is probably masked by mixing due to the water circulation system. However, the conclusion must be that, except possibly under very calm conditions, mechanically generated stress is much more important in nature than convective mixing.

In contrast, the finding of a significant retardation of the exchange rate for oxygen at intermediate wind-speeds under condensing conditions may have considerable environmental importance. Considering the physical processes involved, it is likely that a similar effect will exist for all gases whose air-water transfer is under liquid phase control. Over the oceans there will be on the spatial and temporal average net evaporation from the water surface. However, this does not preclude the existence of certain areas and times for which net condensation will be the dominant process, in particular in coastal upwelling regions where cold, deep water is brought to the surface. Since such areas are often also biologically rich due to the presence of advected nutrients, the retardation demonstrated here for the rate of air-water transfer of oxygen (and other biologically important gases) may well be of environmental significance.

Acknowledgements

For all their help in performing the experiments we would like to thank the members of the scientific and technical staff at IMST, especially P. Bonmarin, J. P. Giovanangeli, J. Quaccia and P. Chambaud. Financial support for the work is gratefully acknowledged from the following organisations: Centre national pour l'Exploitation des Océans (Contracts 77/1673, 78/1869, 79/2003), Natural Environment Research Council, North Atlantic Treaty Organisation (Air-Sea Interaction Committe, Research Grant 1408), the Royal Society (Gassiot Committee).

REFERENCES

Broecker W. S., 1965. An application of natural radon to problems in ocean circulation, in: *Symposium on diffusion in oceans and fresh waters*, edited by T. Ichiye, Lamont Geological Observatory, Palisades, New York, 1965, 116-145.

Broecker H. C., Petermann J., Siems W., 1978. The influence of wind on CO_2-exchange in a wind-wave tunnel, including the effects of monolayers, *J. Mar. Res.*, **36**, 595-610.

Choi I., 1977. Contribution à l'étude des mécanismes physiques de la génération des ondes de capillarité-gravité à une interface air-eau, *Thèse Doct. 3e cycle, IMST, Univ. Aix-Marseille-II*, 59 p.

Coantic M., 1980. Mass transfer across the ocean-air interface: small-scale hydrodynamic and aerodynamic mechanisms, *Phys.-Chem. Hydrodyn.*, **1**, 249-279.

Coantic M., Favre A., 1970. Air-sea interactions: research program and facilities at IMST, in *Proceedings of the 8th symposium on naval hydrodynamics*, Office of Naval Research ARC, **179**, 37-69.

Coantic M., Bonmarin P., Pouchain B., Favre A., 1966. Étude d'une soufflerie pour recherches sur les échanges d'énergie atmosphère-océans, in *Aerodynamics of atmospheric shear flows*, AGARD Conference Proceedings, No. 48, 17-O-17-14.

Deacon E. L., 1977. Gas transfer to and across an air-water interface, *Tellus*, **29**, 363-374.

Downing A. L., Truesdale G. A., 1955. Some factors affecting the rate of solution of oxygen in water, *J. Appl. Chem.*, **5**, 570-581.

Hasse L., Liss P. S., 1980. Gas exchange across the air-sea interface, *Tellus*, **32**, 470-481.

Hoover T. E., 1966. A study of the mechanism of gaseous transfer across an air-water interface using carbon dioxide, *Ph. D. thesis, Texas, A. and M. Univ.*, 114 p.

Hoover T. E., Berkshire D. C., 1969. Effects of hydration on carbon dioxide exchange across an air-water interface, *J. Geophys. Res.*, **74**, 456-464.

Jahne B., Munnich K. O., Siegenthaler U., 1979. Measurements of gas exchange and momentum transfer in a circular wind-water tunnel, *Tellus*, **31**, 321-329.

Kanwisher J., 1963. On the exchange of gases between the atmosphere and the sea, *Deep-Sea Res.*, **10**, 195-207.

Liss P. S., 1973. Processes of gas exchange across an air-water interface, *Deep-Sea Res.*, **20**, 221-238.

Liss P. S., Slater P. G., 1974. Flux of gases across the air-sea interface, *Nature*, **247**, 181-184.

Marmottant B., 1974. Contribution à l'étude de l'évaporation dans une couche limite turbulente d'interface air-eau, *Thèse doct.-ing., IMST, Univ. Aix-Marseille-II*, 92 p.

Monin A. S., Yaglom A. M., 1971. *Statistical fluid mechanics*, MIT Press, Cambridge, Vol. 1, 769 p.

Peng T. H., Broecker W. S., Mathieu G. G., Li Y. H., Baindridge A. E., 1979. Radon evasion rates in the Atlantic and Pacific Oceans as determined during the Geosecs Program, *J. Geophys. Res.*, **84**, 2471-2486.

Pouchain B., 1970. Contribution à l'étude sur maquette d'une soufflerie de simulation des interactions océans-atmosphère, *Thèse doct.-ing., IMST, Univ. Aix-Marseille-II*, 47 p.

Quinn J. A., Otto N. C., 1971. Carbon dioxide exchange at the air-sea interface: flux augmentation by chemical reaction, *J. Geophys. Res.*, 76, 1539-1549.

Resch F. J., Selva J. P., 1979. Turbulent air-water mass transfer under varied stratification conditions, *J. Geophys. Res.*, **84**, 3205-3217.

Selva J. P., 1978. Étude de l'influence de la stratification sur l'évaporation, *Thèse Doct. 3e cycle, IMST, Univ. Aix-Marseille-II*, 166 p, et *Bull. Dir. Étud. Rech. E.D.F.*, ser. **A**, 3, 1979.

Shemdin O. H., 1972. Wind generated current and phase speed of wind waves, *J. Phys. Oceanogr.*, **2**, 411-419.